

A vibrational spectroscopic investigation of the CO+O₂ reaction on Pt{110}

J. H. Miners, S. Cerasari, V. Efstathiou, M. Kim, and D. P. Woodruff

Citation: *J. Chem. Phys.* **117**, 885 (2002); doi: 10.1063/1.1483069

View online: <http://dx.doi.org/10.1063/1.1483069>

View Table of Contents: <http://jcp.aip.org/resource/1/JCPSA6/v117/i2>

Published by the [AIP Publishing LLC](#).

Additional information on *J. Chem. Phys.*

Journal Homepage: <http://jcp.aip.org/>

Journal Information: http://jcp.aip.org/about/about_the_journal

Top downloads: http://jcp.aip.org/features/most_downloaded

Information for Authors: <http://jcp.aip.org/authors>

ADVERTISEMENT



Explore the **Most Cited**
Collection in Applied Physics

AIP
Publishing

A vibrational spectroscopic investigation of the CO+O₂ reaction on Pt{110}

J. H. Miners, S. Cerasari, V. Efstathiou, M. Kim, and D. P. Woodruff^{a)}

Fritz-Haber-Institut der Max-Planck-Gesellschaft, Faradayweg 4-6 D-14195 Berlin, Germany

(Received 24 January 2002; accepted 12 April 2002)

The CO coverage of a Pt{110} surface in both the high and low reaction rate branches of the bistable CO oxidation reaction has been determined by Infrared Reflection-Absorption Spectroscopy (IRAS), first performing extensive calibration experiments on the various factors determining the absorbance and frequency associated with the C–O vibrational stretching mode. The same two states of the surface are shown to be present under steady-state low and high reaction rates and when the surface is undergoing pattern formation and homogeneous reaction rate oscillations. Using the CO coverages determined by IRAS, the intensities observed in a series of photoelectron emission microscopy images have been used to elucidate the oxygen coverage in both coadsorption states. The low reaction rate branch is found to be associated with a high CO coverage (0.5 ± 0.1 ML) and very low O coverage (0.03 ± 0.01 ML) consistent with the (1×1) unreconstructed phase. In the high rate branch the surface has a low CO coverage (0.05 ± 0.03 ML) and O coverages in the range 0.3–0.7 ML [(1×2) reconstructed phase]. No evidence for bridged CO, oxide, or subsurface oxygen, variously proposed to play a role in the reaction rate bistability, was found under the conditions measured. These findings are consistent with the site blocking and reconstruction model. Coadsorption experiments of CO and oxygen under nonreactive conditions, performed as part of the IRAS calibration process, demonstrate that CO and O can occupy a mixed adlayer and identify two different chemical environments for CO adsorption. © 2002 American Institute of Physics. [DOI: 10.1063/1.1483069]

I. INTRODUCTION

The CO+O₂ reaction on Pt{110} (e.g., Refs. 1, 2, and 3) is, after the Belousov–Zhabotinsky reaction, one of the most investigated examples of a chemical system which exhibits kinetic oscillations (e.g., Refs. 4 and 5). It is considered to be an ideal system to study as the reaction is comparatively simple and the reactants can only occupy well-defined positions in a two-dimensional array defined by the crystal surface, thus lending itself to Monte Carlo modeling. Moreover, one has a very good control of the external parameters, being able to maintain and vary accurately the partial pressure of the reactants and the pumping rate, and to sustain a homogeneous temperature over the entire sample.

The essential mechanism of the CO oxidation reaction on metal surfaces is one in which oxygen adsorbs dissociatively and the resulting chemisorbed atomic oxygen reacts with adsorbed CO to form CO₂ which desorbs from the surface. In the case of Pt{110}, the clean surface reconstructs to a (1×2) missing row structure, but this reconstruction is lifted at sufficiently high coverage of CO, but not by atomic oxygen adsorption alone. It is this phase transformation, and associated differences in the activity of the two surface phases, which is believed to be a key factor in the oscillatory CO oxidation rate which can occur on this surface, involving

switching between two reaction branches with different reaction rates.

A large range of nonspatially resolving real-time techniques have been applied to the study of the reaction on this surface including Kelvin probe work function measurement,^{6,7} mass spectrometry,⁷ low energy electron diffraction (LEED),^{7,8} and reflection high energy electron diffraction (RHEED).⁹ More recent measurements with the spatially resolving techniques of photoelectron emission microscopy (PEEM),^{10–12} low energy electron microscopy (LEEM),^{13,14} and mirror electron microscopy (MEM) have shown spatial variations characterized by two distinct states of the surface, believed to correspond to those giving rise to the low and high reaction rates; however, these studies showed that pattern formation may occur even when macroscopic oscillations in the reaction rate are observed in the gas phase. An important consequence of this result is that the information previously gained from the nonspatially resolving techniques concerning oscillatory changes in the state of the surface does not necessarily correspond to the two states observed on a local scale.

While these spatially resolving techniques have greatly increased our understanding of the phenomenology of the spatiotemporal variations involved in this surface reaction, they do not provide any direct measure of the local surface coverage of the reactants. In particular, the relationship between the intensities used to provide the image contrast and the state of the surface is complex. In the case of PEEM, intensity changes are largely related to changes in the work

^{a)} Author to whom correspondence should be addressed. Also at: Department of Physics, University of Warwick, Coventry CV4 7AL, United Kingdom. Electronic mail: d.p.woodruff@warwick.ac.uk

function, but this depends in a complex fashion on the local CO and O coverage and the number of vacant sites. In LEEM the image intensity relates to the intensity of a particular LEED diffracted beam at a specific energy which is influenced not only by whether the surface shows (1×1) or (1×2) periodicity, but also by the degree of local long-range order including the density of surface defects and by the presence of adsorbates. Nevertheless, by measuring LEED intensity-energy spectra under different conditions of surface phase and adsorbate coverage, Meißner *et al.*^{15,16} were able to identify those energies of the incident electron beam for which the LEEM intensity was sensitive primarily to only one of these parameters, e.g., the presence of the (1×1) phase. By recording LEEM images of pattern formation at these voltages, they could show that a chemical wave consisted of a reconstructed part of the surface, and a (1×1) component which was CO covered.¹⁶ Under the conditions used, they found no evidence of faceting. More recent MEM and LEEM measurements of global oscillations (in which the whole surface transforms simultaneously and homogeneously) have indicated that the rate of CO₂ production is lowest when the surface transforms to the (1×1) phase.¹⁵ Despite these achievements, however, there is still only indirect information concerning the nature and concentration of the chemical species on the surface during the oscillation, and their relation to the rate of reaction. Many models have been proposed to explain the behavior in this system, but in the absence of this basic information all of these models are necessarily somewhat speculative.

Among the processes considered to be responsible for the bistability and hysteresis of this reaction system are the lifting of the surface reconstruction,¹⁷ CO site blocking of oxygen dissociation,^{18,19} changes of the CO bonding coordination site, defect formation and the faceting of the surface,⁸ subsurface oxygen formation,^{20,12} oxide formation,²¹ and carbon formation.²² It should be noted that the latter two processes do not occur on single crystal surfaces at pressures below 10^{-4} mbar.²² The influence of reconstruction and site blocking are currently thought to be the key mechanisms determining the behavior at low temperatures and pressures.

A clear resolution of the mechanisms creating the novel properties of this reaction requires experimental determination of quite a large number of variables. Specifically, one needs to know the correlations between (i) the state of the surface order, notably whether it is (1×1) or (1×2) , but also whether it is faceted or heavily defected; (ii) the CO coverage; (iii) the CO site occupation; (iv) the oxygen coverage, and (v) the rate of reaction.

In this paper we present the results of a real-time infrared reflection-absorption spectroscopy (IRAS) investigation which we show can be used to obtain the local CO coverage both under steady state reaction conditions and during kinetic oscillations and pattern formation. Concurrent mass spectrometry measurements allow us to relate the CO coverage to the rate of CO₂ production. The IRAS data are also sensitive to the bonding configuration of the CO and the presence of surface oxygen. We have also reproduced these experiments in a PEEM instrument, and armed with the knowledge of the CO coverage from the IRAS study, it is

possible to use the PEEM image intensity to deduce the oxygen coverage. By combining the results from these measurements and from a parallel LEEM/LEED investigation conducted in this laboratory,^{15,16} and relating them via the rate of CO₂ production, we can obtain a full description of this system.

II. EXPERIMENTAL DETAILS AND METHODOLOGY

The instrument used in these experiments has been described previously.²³ Briefly, it consists of a commercial FTIR spectrometer (Biorad FTS-60A/896) modified for operation under low vacuum ($\sim 1 \times 10^{-3}$ mbar) interfaced to a UHV chamber equipped with rear-view LEED optics, a movable quadrupole mass spectrometer and facilities for argon ion sputtering. Spectra were recorded using a liquid nitrogen-cooled narrow-band MCT detector. The same Pt{110} crystal and preparation techniques were used as in the earlier LEEM experiments.^{15,16} The sample was mounted on a liquid nitrogen-cooled cold finger and could be resistively heated such that temperatures between 85 K and 1500 K could be maintained to a stability of 0.05 K. The temperature was measured using a *K*-type thermocouple spot-welded directly to the top of the crystal and the signal from this thermocouple was fed back into the computer-controlled temperature control unit. The sample gases used in the experiments are of the highest commercially available purity: 99.997% for CO, (Linde), 99.999% for O₂ (Messer-Griesheim). The partial pressures quoted in each experiment have been corrected for the different ion gauge sensitivities of the respective gases, i.e., $S_{\text{CO}}/S_{\text{N}_2} = 1.0$ and $S_{\text{O}_2}/S_{\text{N}_2} = 0.8$ were used as correction factors. The UHV chamber routinely obtains a base pressure of 1×10^{-10} mbar. The crystal was cleaned prior to each experiment via oxygen treatment at 800 K followed by repeated cycles of argon ion bombardment at 750 K and annealing at 1100 K.

The infrared absorption band of an adsorbed species can be described in terms of four parameters (i) the center frequency, (ii) the integrated absorbance, (iii) the full width at half maximum (FWHM), and (iv) the peak shape. Each of these components can provide information on the coverage and local environment of the adsorbate under investigation as follows:

- (i) Changes in the center frequency of the vibrational mode of an adsorbed species can occur as a result of four distinct effects; these are changes in the adsorption site, variations in the chemical shift, the extent of the dynamic dipole-dipole coupling, and the degree of dephasing.²⁴ The chemical shift (a change in the vibrational frequency due to a change in the electronic interaction of the molecule with its environment) may vary as a result of changes in the local adsorbate environment (including coverage and substrate order). The extent of dynamic dipole-dipole coupling is determined by the local coverage of adsorbate molecules with similar vibrational frequencies.^{25,26} These components can be separated by performing appropriate calibration experiments. Specifically, the frequency shift due to dipole-dipole coupling can be identified

by performing isotopic dilution measurements, while the influence of the dephasing component can be established through its temperature dependence.

- (ii) The integrated absorbance of an infrared band provides information on the coverage of the associated species, but this may not increase linearly with coverage²⁴ and the absorption cross-section changes with molecular orientation and adsorbate coordination.²⁷ Proper interpretation of measurements of the absorbance is therefore also dependent on careful calibration experiments.
- (iii) The width of an infrared absorption peak can vary with temperature due to dephasing, and may also contain a component arising from inhomogeneity in the adlayer; disorder results in a variety of frequencies of absorbers and hence a peak broadening.
- (iv) The relative importance of these two contributions to the broadening, "lifetime" and inhomogeneity, may be determined by the peak shape; if lifetime broadening is dominant one expects a Lorentzian shape, whereas inhomogeneities lead to a Gaussian line shape.²⁸

In order to exploit as much as possible of this more detailed information from the IRAS measurements of the C–O stretching vibrations from a Pt{110} surface under CO oxidation reaction conditions, a series of calibration experiments involving CO and oxygen adsorption were first carried out under static conditions. The results of these measurements are reported here in Sec. III.

While IRAS can provide us with considerable quantitative information on the local and average CO coverage on the surface during the reaction and provide clear evidence for the presence and absence of coadsorbed O in the two states, they do not allow us to quantify the oxygen coverage. PEEM, on the other hand, is much more sensitive to the surface concentration of oxygen and thus provides complementary information, so additional experiments were performed using this technique. The PEEM experimental setup used here has been described in detail elsewhere,^{29–33} and the same sample cleaning procedures were applied to the crystal as in the IRAS experiments. The intensities seen in a PEEM image are primarily determined by the variations in work function which in turn depend on the coverage of CO and oxygen; these relationships have been previously calibrated.^{30–33} If the CO concentration is known independently from IRAS, its contribution to the PEEM intensity can be calculated and the measured PEEM intensity can then be used to determine the oxygen coverage.

III. IRAS CALIBRATION STUDIES

A. CO adsorption on Pt{110}

The clean Pt{110} surface is reconstructed into the (1×2) missing-row phase.³⁴ CO adsorption at temperatures below 250 K occurs without lifting the reconstruction.³⁵ At temperatures greater than 250 K, however, LEED and STM studies have shown that, on reaching an average coverage of 0.2 ML, CO-induced homogeneous nucleation of

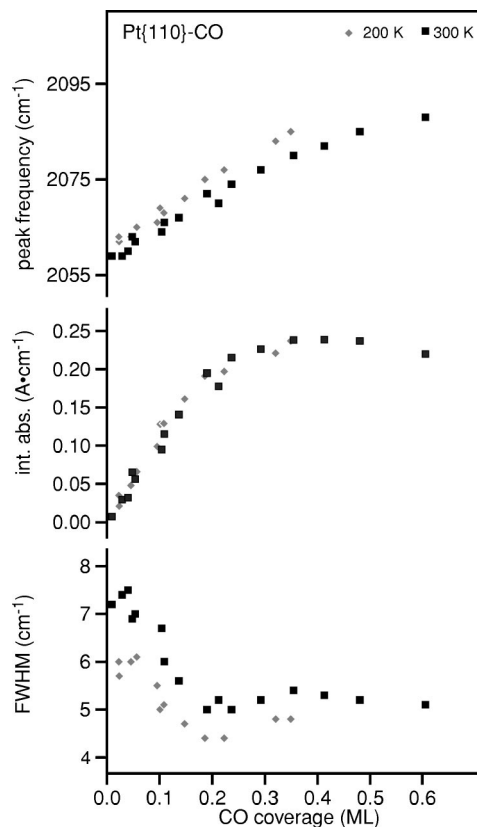


FIG. 1. Graph of the main quantitative features of the C–O stretching band seen in IRAS as a function of CO coverage on Pt{110} at sample temperatures of 200 K (light gray) and 300 K (black squares).

the (1×1) phase occurs and the reconstruction is lifted.^{36,37} The value of the C–O stretching frequency in vibrational spectroscopy indicates that CO adsorbs in an atop configuration, and a saturation coverage of 1 ML can be obtained by slowly cooling a clean Pt{110},^{38,39} from 700 to 300 K, in an ambient pressure of 1×10^{-7} mbar CO.^{35,40}

Hayden *et al.* have used IRAS and temperature-programmed desorption (TPD) to measure the coverage dependence of the C–O stretching frequency on Pt{110} at a surface temperature of 300 K.³⁸ By diluting the ¹²CO in ¹³CO, they were able to show that all coverage-dependent changes in the frequency of the mode were due to dipole–dipole coupling, and that there is no coverage-dependent chemical shift on this surface. Furthermore, since the surface changes phase from (1×2) to (1×1) during the absorption sequence, there is evidently no chemical shift associated with this surface phase transition. These experiments also showed that the absorption cross section of the IRAS band associated with the C–O stretching frequency decreases after a coverage of 0.5 ML has been reached. They assigned this to the tilting of the CO molecule at higher coverages, a conclusion confirmed by angle-resolved ultraviolet photoelectron spectroscopy (ARUPS),⁴¹ XPS and XPD,⁴² and reproduced by extended Hückel molecular orbital calculations.⁴³

Figure 1 shows the results of our first calibration experiment in which we measured the coverage dependence of the C–O internal stretching vibration at sample temperatures of 200 and 300 K. These results are clearly consistent with

those of Hayden *et al.*, albeit at higher spectral resolution. The coverages were determined by TPD, using the saturation 1 ML CO phase formed as described above as our calibration point. At 200 K the CO-induced unreconstruction of the (1×2) phase is suppressed and the surface retains the (1×2) ordering, whereas at 300 K the $(1 \times 2) \rightarrow (1 \times 1)$ transition occurs with increasing CO coverage, yet there are only small differences between the two plots, confirming the earlier finding of the experiments conducted only at 300 K that the surface structural phase has little effect on the absorption cross section of the IRAS band. Notice that the detailed measurements at the lower temperature shown here only extend to 0.35 ML, but this is already much higher than the coverage needed at room temperature to induce the structural phase transition (0.2 ML). Additional measurements at 1 ML coverage at both temperatures confirmed the essential equivalence of the IRAS spectra at the two temperatures over the full coverage range. As is shown below, the slightly higher frequency and smaller FWHM observed at 200 K, is attributable to less dephasing; at 200 K there is less thermally induced occupation of low-frequency (frustrated translational) modes that are coupled to the C–O stretching mode.²⁶

One issue in the interpretation of these IRAS data is the role of CO island formation. At 200 K on the (1×2) surface the observed linear dependence of the frequency on coverage is consistent with the effect of dynamic dipole–dipole coupling in the absence of islanding.^{25,26,44,45} At 300 K the surface transforms to the (1×1) phase as the average CO coverage increases above 0.2 ML. If this process were to proceed with a significantly higher CO coverage on the (1×1) islands than on the surrounding (1×2) surface one would observe two distinct IRAS peaks at intermediate average coverages for a sample temperature of 300 K. This is not observed, and indeed no significant difference is observed in the coverage dependence of the frequency between the measurements taken at sample temperatures of 200 and 300 K, for coverages between 0.2 and 0.5 ML. This is consistent with the observation by STM that at 300 K the phase transition occurs by homogeneous, rather than heterogeneous nucleation, and that increasing CO coverage leads to an increase in the density, rather than the size, of the (1×1) islands,³⁷ but also shows that the local and average CO concentrations all over the surface are essentially the same. On this basis we will assume that the ordinate of Fig. 1 does represent local coverage and, combined with measured frequency shift due to dipole–dipole coupling, we will therefore use the C–O stretching frequency to determine the local coverage under reaction conditions. Knowing the cross section for adsorption at this local coverage, one can also use the integrated absorbance to determine the total coverage.

The higher resolution of our measurements,^{27,38,46,47} and the use of absorbance $[\log(I_0/I)]$ as opposed to transmission (I_0/I) in the presentation of the spectra, allows small variations in spectral line shape to be observed and interpreted in a more meaningful fashion. The slight increase in the FWHM (full width at half maximum) with increasing coverage at very low coverage is as expected from dipole–dipole coupling.²⁶ Inspection of the original IRAS spectra also shows that the absorption peak has a Lorentzian line shape,

indicating that the width is attributable to homogeneous rather than inhomogeneous broadening.²⁸ Finally, we should note that our data show no evidence of any bridging CO that would be expected to give rise to a significantly lower C–O stretching frequency in the 1800–1900 cm^{-1} range. This is in agreement with recent XPS and XPD measurements in which bridging CO is only observed at the high coverage of $\theta_{\text{CO}} = 1.09$ ML which can only be obtained by cooling down the crystal from 600 K to $T < 240$ K in ambient CO.⁴²

This initial calibration experiment provides characterization of the IRAS for CO on Pt{110} at sample temperatures of 200 K and 300 K, but we wish to study CO on this surface at the significantly higher temperatures at which CO oxidation reaction oscillations occur. At these higher temperatures we must account for the changes in the spectra due to dephasing; i.e., the variations in the C–O stretching frequency due to coupling to lower frequency frustrated translational vibrational modes, which become occupied to a significant degree at higher temperatures.^{48–51} Two approaches to this problem are possible. The first is to measure the temperature dependence of the IRAS data at constant coverage (and thus at constant dipole–dipole coupling); in this experiment one also obtains information on the temperature dependence of the FWHM. A limitation to this method is that thermal desorption of CO becomes significant at temperatures above 350 K. The alternative method is to eliminate dipole–dipole coupling by diluting the ^{12}CO in ^{13}CO . Since it is already established that there is no coverage-dependant chemical shift in this system, changes in coverage in the absence of dynamic dipole coupling will have no effect on the frequency, and all temperature-dependent variation will then be due to dephasing. This method can be applied at higher temperatures (and lower associated coverages).

Figure 2 summarizes the results of both of these experiments. In one experiment we prepared a 1 ML coverage of CO and varied the temperature in an ambient pressure of 2×10^{-7} mbar CO. The temperature was raised from 150 K to 500 K, in steps of 25 K, and spectra comprising 256 scans at a resolution of 2 cm^{-1} were recorded. The maximum temperature at which the saturated 1 ML CO coverage could be maintained under this pressure of CO was 350 K. This was deduced by subsequently raising the CO pressure to 1×10^{-5} mbar and noting that there was a change in the IRAS spectra for $T > 350$ K. The results of these experiments showed no change in integrated absorbance with increasing temperature. Increasing the temperature from 150 to 350 K led to a decrease in the center frequency of the C–O stretching band by $7 \pm 2 \text{ cm}^{-1}$. The form of the observed changes in both the peak width and center frequency are as expected due to dephasing and the peak shift is of a similar magnitude to that seen on Pt{111}.^{24,51,52} Since there is very little change in the FWHM of around 5 cm^{-1} when the CO coverage, θ_{CO} , increases beyond a value of 0.2 ML (see Fig. 1 and Refs. 37, 46, 47, and 27), we should note that for a surface exposed to 2×10^{-5} mbar CO at 500 K the IRAS peak showed a Lorentzian form with a FWHM of 7.8 cm^{-1} .

It is interesting to note the 4 cm^{-1} difference shown in Fig. 2 between the center frequency values obtained from the isotopic dilution experiments (full line) and the extrapolated

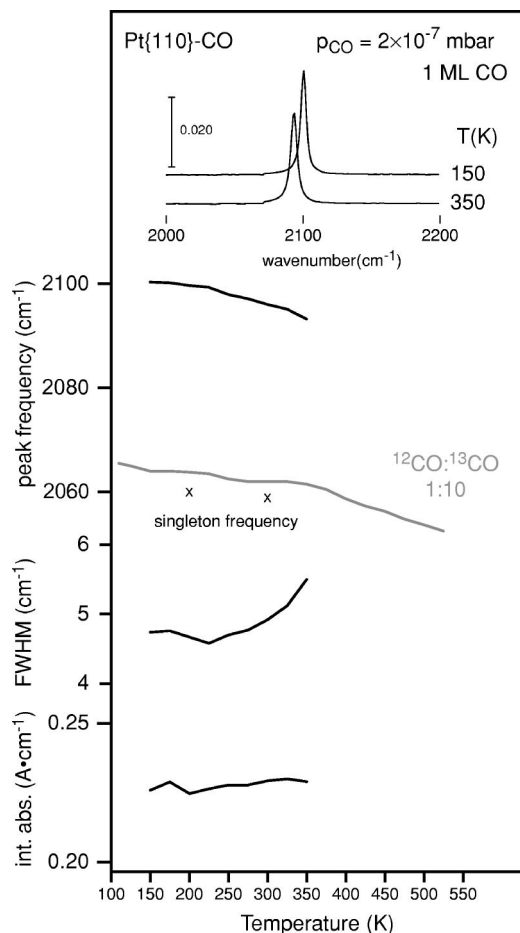


FIG. 2. The temperature dependence of IRAS of 1 ML CO coverage on Pt{111}. The two spectra at the top and the bold lines all relate to pure ¹²CO layers. The light line corresponds to data collected with a mixture 1:10 ¹²CO:¹³CO. The singleton (extrapolated zero coverage) frequencies at 200 and 300 K (crosses) are also depicted.

zero-coverage (singleton) values at 200 and 300 K, shown as the two crosses. This arises because, for a total coverage of 1 ML and a 1:10 isotopic ratio ¹²CO:¹³CO, the local coverage of ¹²CO is 0.1 ML, sufficient to give rise to a small but significant dipole–dipole coupling shift. As may be seen in Fig. 1, this coverage does lead to a shift due to dipole–dipole coupling of precisely this value of 4 cm⁻¹. Notice also, in Fig. 2, that the pronounced fall in the center frequency at higher temperatures (>350 K) seen in the results from the isotopic dilution experiment is also largely attributable to this same effect, the total CO coverage (and thus also the ¹²CO coverage) falling at high temperatures.

Using the results of this experiment, we are able to account for the temperature induced change in the singleton frequency, and thus relate spectra of CO on Pt{110} recorded at any temperature between 150 and 525 K to the calibration measurement at 300 K, with an accuracy of ± 2 cm⁻¹. From the dipole–dipole coupling shift one can then determine the local CO coverage.

B. CO coadsorption with oxygen under nonreactive conditions

While the calibration experiments on pure CO adsorption show no chemical shifts associated with the substrate

phase changes, or electronic CO–CO interactions, our objective is to apply IRAS to a study of the CO/O interaction under reaction conditions, so we must also characterize any possible chemical shift in the C–O vibrational frequency due to the presence of coadsorbed oxygen. Indeed, it is known from other systems that oxygen has a strong, repulsive interaction with CO, resulting in island formation and a chemical shift of the C–O stretching frequency.^{52–55}

Oxygen adsorption on Pt{110} is dissociative at temperatures above 175 K.⁵⁶ It requires, therefore, two vacant adsorption sites to adsorb. In contrast to CO, oxygen adsorption does not result in the lifting of the (1×2) reconstruction.⁴⁰ Furthermore, although CO has a sticking coefficient of 1.0 on both surface phases,³⁵ the sticking coefficient of O is estimated to be 0.4 and 0.6 on the (1×2) and the (1×1) phase, respectively.⁵⁷ There are no conventional quantitative structure determinations for the local adsorption geometry of either CO or O on Pt(110), and most of the models in the literature are largely speculative. In the case of oxygen adsorption on Pt{110}(1×2) such speculation favors the threefold coordinated hollow sites on the (111)-type walls of the troughs, although at low coverage occupation of the fourfold coordinated hollow sites located at the bottom of the <110> troughs has been proposed.^{56–58} A recent investigation using a combination of STM and density functional theory (DFT) calculations, on the other hand, strongly favors the (111) nanofacet threefold coordinated hollow sites over these trough sites.⁵⁹ In the case of CO adsorption an early suggestion was that these trough hollow sites were occupied by CO at low coverage, but that bridge sites on the top of the rows may be occupied at saturation coverage.³⁵ However, the fact that the C–O stretching frequency is always above 2000 cm⁻¹ has been generally taken as a more reliable indication that local atop sites are always occupied by this species; the fact that the saturation coverage of 1 ML is the same on the (1×2) and (1×1) surfaces (at low and higher temperatures, respectively) is also thought to imply that on the (1×2) phase CO must occupy local atop sites in the troughs as well as on the ridges.²⁷

In the absence of adsorbed oxygen, the adsorption of CO on a clean Pt{110}(1×2) surface at low coverage is homogeneous as discussed above. In the presence of oxygen, however, not only could interaction of the coadsorbed species lead to a change in the local site occupied by the CO, but one may now have island formation with significant implications for the macroscopic reaction of the two species.⁶⁰ A separation of CO and O into distinct islands could also strongly influence the ability of the two species to react, and perhaps explain the origin of poisoning effects observed under reaction conditions.¹⁹ In order to interpret the IRAS measurements under reaction conditions it is therefore important to first study the effects of coadsorption of oxygen and CO under nonreaction conditions.

The results of the first of these coadsorption calibration experiments are shown in Fig. 3; in the lower part of the figure IRAS data are shown from a surface predosed with 0.2 L CO at 300 K, and then exposed to increasing doses of molecular oxygen. The presence of the coadsorbed O following a 2 L dose leads to an upward frequency shift and to

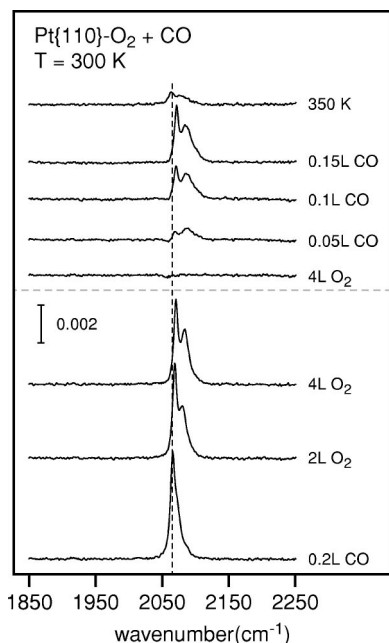


FIG. 3. Two sets of IRAS spectra obtained from Pt{110} following the coadsorption of CO and oxygen at 300 K. The lower group of spectra were obtained by first adsorbing CO and then oxygen; this exposure sequence was reversed to obtain the upper group of spectra.

splitting of the band into components at 2069 and 2088 cm^{-1} from its previous value of 2061 cm^{-1} . No CO_2 was produced. Further oxygen exposure results in a small increase in the frequency of both bands. In the upper part of Fig. 3 are shown the results of a similar experiment in which the order of gas dosing was reversed, a predose of 4 L O_2 being followed by successive dosing with CO. Again two distinct C–O vibrational bands appear at similar energies to those described above, while increasing CO exposure results in increasing amplitudes of the bands at constant frequencies. Heating the surface to 350 K results in the partial reaction of CO with O. Note that the chemisorbed oxygen can only be removed by total reaction with CO at temperatures in excess of 400 K, or by sputtering; heating an oxygen covered surface to 1000 K followed by dosing with CO yielded a similar two-peak C–O vibrational spectrum characteristic of O/CO coadsorption. No C–O stretching frequency in the 1800–1900 cm^{-1} range, characteristic of a bridging CO species, was observed in either experiment.

There are two possible ways in which the coadsorbed O could give rise to the upward shift of the C–O vibrational frequency. One of these is that O–CO repulsion could lead to isolated CO island formation; the shift would then arise from dipole–dipole coupling in the islands which would have a higher local coverage than in the absence of this O–CO repulsion. The alternative explanation is that the increase in vibrational energy is due to an O-induced chemical shift. Of course, it is also possible that *both* of these effects may contribute to the observed phenomena. In order to distinguish these processes, experiments similar to those leading to the results of Fig. 3 were repeated using isotopic mixtures of CO, and the results are shown in Fig. 4. Notice that the spectra are complicated slightly by the presence of a feature

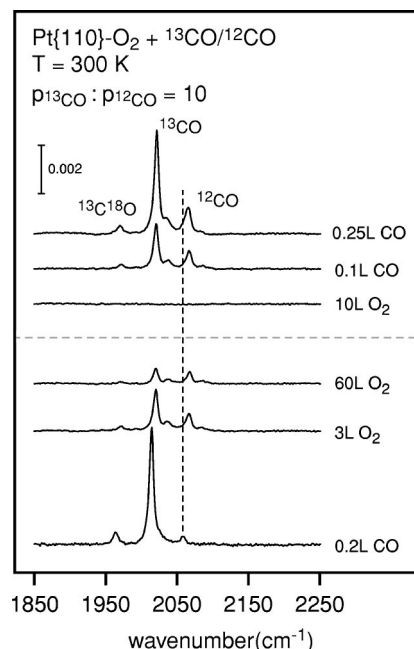


FIG. 4. Two sets of IRAS spectra obtained from Pt{110} following the coadsorption of CO and oxygen at 300 K using an isotopic mixture of 1:10 $^{12}\text{C}^{16}\text{O}$: $^{13}\text{C}^{16}\text{O}$. Otherwise similar to Fig. 3.

around 1960 cm^{-1} associated with a component of $^{12}\text{C}^{18}\text{O}$ in the gas mixture, which was nominally only of $^{12}\text{C}^{16}\text{O}$ and $^{13}\text{C}^{16}\text{O}$; however, this is well removed from the spectral region of interest and the behavior of this species actually reinforces the primary results described below. We have already noted that, using a 1:10 isotopic ratio of $^{12}\text{C}^{16}\text{O}$: $^{13}\text{C}^{16}\text{O}$, the frequency shift due to dipole–dipole coupling in the peak associated with the $^{12}\text{C}^{16}\text{O}$ species can be no more than 4 cm^{-1} (its maximum value at saturation coverage). As may be seen in Fig. 4, however, the lowest oxygen exposure to a surface predosed with this mixture of CO isotopes immediately leads to an upward shift and a splitting of not only the $^{13}\text{C}^{16}\text{O}$ -related peak, but also of that associated with $^{12}\text{C}^{16}\text{O}$ from the singleton value of 2058 cm^{-1} to 2066.7 and 2084 cm^{-1} . Identical frequencies are observed on reversing the dosing sequence, and it is clear that the magnitude of the shifts is the same for the majority and minority CO species. We therefore conclude that the entire change in frequency due to O coadsorption observed in Fig. 3 is due to an O-induced chemical shift, and not to dipole–dipole coupling. This means that we can exclude the possibility of CO island formation induced by the coadsorbed O.

While these experiments clearly identify the mechanism of the upward frequency shift induced by the coadsorbed O, a question remains as to the origin of the splitting into two bands. Notice that the low CO coverages (<0.2 ML) used in these experiments are insufficient to initiate nucleation of the (1×1) phase, so the two bands cannot be associated with CO adsorbed on the two different surface phases of Pt{110}. Similarly, while there have been suggestions in the literature of subsurface oxygen species or local oxide formation during CO/ O_2 reaction conditions over Pt{110}, we can exclude the local interaction of some of the CO with one of these species as the origin of a second band; conversion of O to subsurface

oxygen can only be achieved by prolonged exposure at 400 K.¹² There is also rather clear evidence that true oxide cannot be formed on Pt at the low pressures relevant to these experiments,^{61,62} but as CO adsorption upon the oxidized surface is known to have a characteristic frequency of 2120 cm⁻¹ (Refs. 63 and 64) which is not observed here, we can clearly discount this possibility. We must therefore conclude that CO and O can form a mixed chemisorbed adlayer on the (1×2) reconstructed surface in which there are two CO species which differ in some way.

Bearing in mind that chemical shifts in vibrational spectroscopy arise from a local electronic effect, one possible explanation for two bands would be that the upper band corresponds to CO molecules adsorbed in sites with O near neighbors, while the lower energy band arises from CO molecules which are relatively isolated from adsorbed O atoms. If this were the case, however, the relative intensities of the two bands would be dependent on the relative coverages of adsorbed O and CO. For example, for a low CO coverage, increasing the O coverage should transfer intensity from the lower (isolated CO) band to the higher energy (O neighboring) band. Apart from the spectrum recorded at the lowest CO exposure after oxygen predosing, Figs. 3 and 4 indicate there is essentially no variation in the relative intensities of the two bands, implying that this hypothesis is not correct.

The alternative explanation for the two bands is that they correspond to two different local adsorption configurations of CO which have different O-induced chemical shifts, effectively implying that there are two inequivalent sites for CO adsorption relative to the position of the coadsorbed O atoms. In the absence of any hard information concerning the adsorption geometries of either coadsorbate, expanding on this idea is necessarily somewhat speculative. We note, however, that the values of the C–O stretching frequencies clearly favor all CO molecules being in local atop sites, and that on the (1×2) reconstructed phase we have already remarked that, at least at high coverages, this must imply atop adsorption on both ridge and hollow Pt atoms. If the O atoms do occupy (hollow) sites on the (111) trough walls as seems to be favored by the only real attempt to establish the oxygen adsorption site,⁵⁹ one might then imagine that these two distinct CO sites would suffer different O-induced chemical shifts, and could account for the two vibrational bands observed.

IV. CO+OXYGEN COADSORPTION UNDER REACTION CONDITIONS

A. IRAS

Two distinct regions of kinetic behavior have been identified in the reaction of CO+O₂ on Pt{110}. Bonzel and Ku^{18,19} observed that, for a given temperature and oxygen pressure, the rate of CO₂ production initially increased as the partial pressure of CO increased up to a critical value, whereupon the rate rapidly decreased. They were able to model this behavior by considering that adsorbed CO molecules block sites for oxygen absorption, but not vice versa. This model was supported by their observation that an oxygenated surface can react immediately when it is exposed to CO, but

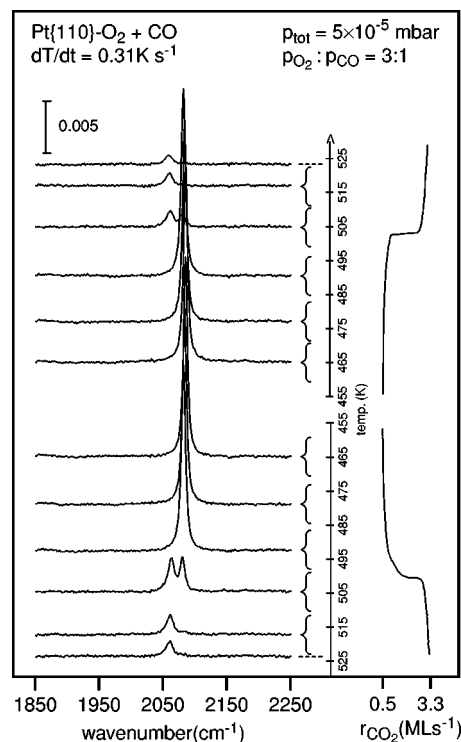


FIG. 5. The IRAS spectra (left) and the rate of CO₂ production (right) recorded continuously while a Pt{110} surface, exposed to a partial pressure of 3.8×10^{-5} mbar O₂ and a 1.3×10^{-5} mbar CO, was heated and cooled at a rate of 0.31 K s^{-1} . Each spectrum was recorded at a resolution of 2 cm^{-1} and required 45 s to acquire.

when the dosing sequence is reversed and a coverage CO is prepared, an induction period is required (presumably during which CO desorption is occurring) before reaction can occur ($475 \text{ K} < T < 595 \text{ K}$).¹⁸ However, as stated in the introduction, a variety of other models can also describe this behavior. The bifurcation in the reaction rate exhibited by CO oxidation over Pt{110} has subsequently been well documented. The high rate branch is associated with a higher temperature and a greater O₂:CO partial pressure ratio.^{1,6,7,19,65} It is known that the surface is in the (1×2) state during the high rate branch and in the (1×1) state in the low rate branch.^{16,65} There are, however, no experimental data available which identify the nature and coverage of the surface species during either rate branch.

Figure 5 displays IRAS spectra and mass spectroscopy (MS) measurements recorded concurrently while the temperature of a Pt{110} crystal, exposed to a constant flow of oxygen and CO, was successively lowered and raised. The rate of CO₂ production in this figure is expressed in ML s⁻¹, calibrated by preparing a surface with 1 ML of adsorbed CO at 300 K and then warming the crystal in 3.75×10^{-5} mbar O₂ while recording the CO₂ and CO partial pressures. The measurements of Fig. 5 show a small hysteresis in the temperature at which the transition between the two rate branches occurs on cooling (500 K), and heating (504 K). Two vibrational bands are observed, one associated with each of the two reaction rate states. A high intensity band at $\sim 2085 \text{ cm}^{-1}$ is seen in the low rate branch with a FWHM of 7.7 cm^{-1} and a Lorentzian line shape associated with life-

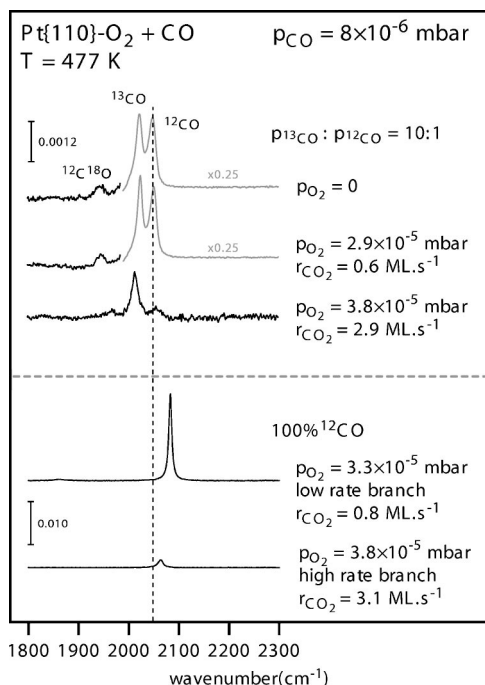


FIG. 6. The IRAS spectra from Pt{110} recorded under reaction conditions at constant temperature and a CO partial pressure of 8×10^{-6} mbar, but with varying partial pressure of O. The associated rates of CO₂ production are also noted. In the upper set of spectra, a mixture 1:10 ¹²CO:¹³CO was used.

time broadening.²⁸ The high rate branch is characterized by an absorption band at lower frequency (~ 2062 cm⁻¹) with a FWHM of 12 cm⁻¹ and Voigt line shape (of which 8 cm⁻¹ is Lorentzian). The difference in frequency of the two bands arises from a combination of dynamic-dipole coupling with increasing CO coverage and the effect of O coadsorption producing a chemical shift. These can be separated by using isotopic mixtures as described below. No IRAS band associated with the presence of either CO adsorbed in the bridge configuration (around 1800 cm⁻¹) or CO adsorbed on an oxide surface (2120 cm⁻¹) was observed.

The local CO coverage in these two states can be deduced from the shift due to dipole-dipole coupling, and the local chemical environment from the chemical shift. The results of experiments to separate these components are shown in Fig. 6. In order to keep any spectral shift due to dephasing constant during this experiment, the system was kept at constant temperature and the system varied from high rate branch to low rate branch by varying the oxygen partial pressure while maintaining the CO partial pressure constant. In the lower half of the figure are the spectra for the high and low rate branch using 100% ¹²CO (cf. Fig. 5), while the upper half of the figure shows the results of repeating the experiment using an isotopic mixture of ¹³CO and 10% ¹²CO. In the uppermost spectrum, recorded in the absence of oxygen, the isotopically diluted ¹²CO band is centered at a frequency of 2051 cm⁻¹. This value corresponds to the frequency of a band with no chemical shift and a maximum of 4 cm⁻¹ dipole-dipole shift.

The IRAS band associated with the high rate branch is observed at a frequency of 2062 cm⁻¹, with an integrated

absorbance of 0.025 A cm⁻¹. When using isotopic dilution it has a frequency of 2056 cm⁻¹. We can therefore conclude that the frequency of 2062 cm⁻¹ includes a shift due to dipole-dipole coupling of 6 ± 3 cm⁻¹, while accounting for the temperature dependence of the C-O stretching frequency shown in Fig. 2 indicates that there is also a chemical shift of 5 ± 2 cm⁻¹ indicative of coadsorption with oxygen. Figure 1 also allows us to equate the dipole-dipole coupling shift to a local CO coverage of 0.05 ± 0.04 ML. The large Gaussian component in the broadening of this band implies inhomogeneous broadening and is indicative of a large number of adsorbate environments for the CO, as would be expected of a steady state CO coverage, in a mixed O-CO adlayer. This intermixing is confirmed by a determination of the average CO coverage from the measured integrated absorption (using the cross section of CO at this CO local coverage); the value obtained is 0.025 ML. Despite the limited precision of the local coverage determination, it is clear that these two values of the local and average coverage are most obviously reconciled by a fully intermixed rather than islanded CO layer. The rather accurate determination of the average CO coverage as a low value of 0.025 ML clearly implies, from earlier LEED studies, that the surface in this high rate branch of the reaction is in the (1 × 2) reconstructed phase.⁶⁵

The IRAS band associated with the low rate branch is observed at a frequency of 2083 cm⁻¹, with an integrated absorbance of 0.211 A cm⁻¹. When using isotopic dilution it has a frequency of 2051 cm⁻¹. Indeed the IRAS band associated with the low rate branch is identical to that obtained in the absence of any O₂ in the gas phase. The shift of 32 ± 3 cm⁻¹ due to dynamic dipole coupling yields a value for the local CO coverage of 0.5 ± 0.1 ML while comparison with the average coverage obtained from the integrated absorbance shows that this average coverage is present on $90 \pm 10\%$ of the surface; i.e., there is no islanding. This coverage means that there can be no pairs of adjacent vacant sites upon which O₂ can dissociatively adsorb, thus providing the first direct evidence that the low rate branch corresponds to a CO-poisoned surface. Prior LEED studies indicate that at this CO coverage the surface is in the unreconstructed (1 × 1) phase.⁶⁵

It is expected that the two states observed in the bifurcation of the reaction rate are the same two states which coexist on the surface during pattern formation. Nevertheless, we may ask whether our IRAS experiments correspond to the situation of homogeneous switching of the surface between these two states or pattern formation. Figure 5 contains two spectra in which the C-O stretching bands characteristic of both of the two states are observed, but this does not prove that the two states are present on the surface at the same time as would be the case in pattern formation; an alternative explanation is that the entire surface switched from one state to the other during the time taken to accumulate these spectra.

To provide further information on this aspect, kinetic rate oscillations were established and monitored simultaneously by time-resolved IRAS and mass spectrometry. A representative set of IRAS spectra and the associated CO₂ production rate derived from the mass spectrometry are dis-

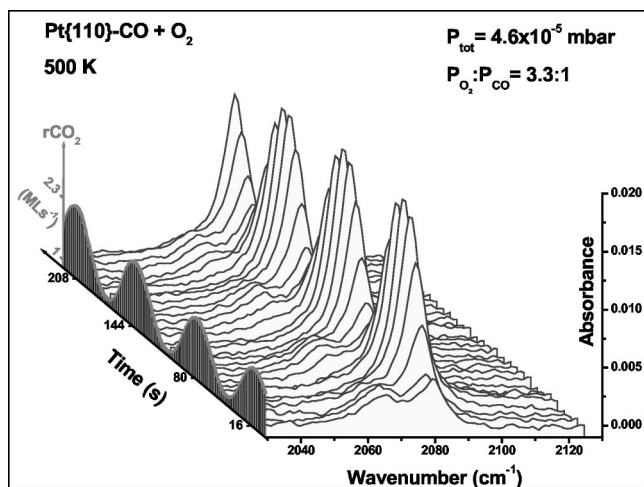


FIG. 7. A set of IRAS spectra recorded from Pt{110} under conditions giving rise to an oscillating reaction rate with a period of 63 seconds. The spectra were recorded with 7.2 s temporal and 2 cm⁻¹ spectral resolution. Also shown is the CO₂ production rate obtained from monitoring the mass 44 partial pressure on the mass spectrometer.

played in Fig. 7, while the amplitudes of the main IRAS and mass spectrometer peaks are shown as a function of time in Fig. 8. The oscillations in the mass spectrometer signals clearly show that a macroscopic kinetic oscillation in the reaction rate is occurring. In addition, however, the IRAS data show the presence on the surface of the same two states which are observed on either side of the reaction rate bifurcation. The fact that both IRAS bands are present at approximately constant frequency throughout the oscillations, but change their relative intensities, indicates that the two associated species are spatially separated; they coexist on different parts of the surface but with the relative areas of the

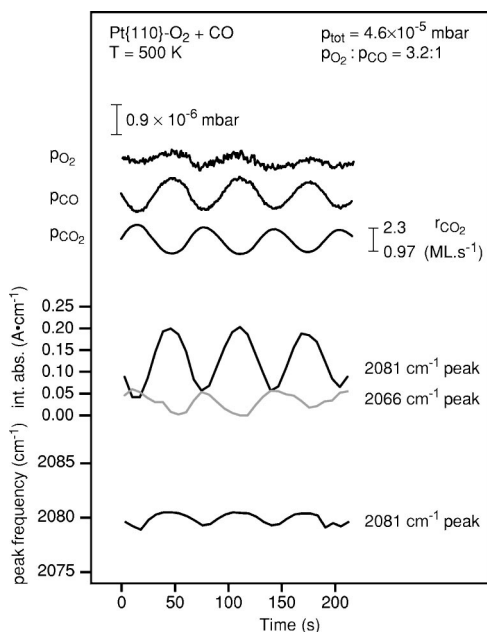


FIG. 8. Summary of the main results of the experiment shown in raw data form in Fig. 7, notably the temporal variation of the partial pressures of O₂, CO, and CO₂, the integrated absorbance of the two IRAS bands and the exact frequency of the IRAS peak around the 2081 cm⁻¹ band.

surface in each state oscillating with time, thus indicating that microscopic local pattern formation is occurring. The macroscopic reaction is presumably coupled either via the gas phase or faceting.^{15,65,66} Similar measurements of oscillations were recorded under a wide range of conditions (450 K < T < 530 K, 1 × 10⁻⁵ mbar < p_{total} < 1 × 10⁻⁴ mbar) with periods from seconds to minutes, and all of these exhibited the behavior shown in these two figures. Notice too that Fig. 8 shows particularly clearly the in-phase behavior of the CO₂ partial pressure and the 2066 cm⁻¹ vibrational band, and the fact that the 2081 cm⁻¹ band has an intensity which is in antiphase to this monitor of the reaction rate, providing a particularly clear correlation of these monitors of the surface state with the rate of reaction.

Note that in these experiments the pumping speed was high, ensuring that that the measured partial pressures in the gas phase relate directly relate to the rate of reaction or production. Furthermore, the oscillations in the pressure of the product CO₂ are exactly out of phase with those of the reactants, CO and O₂. The highest rate of production of CO₂ thus occurs when the rate of adsorption of the reactants is highest, which indicates that the high rate branch in the oscillation reaction is occurring by adsorption and *immediate* reaction on the surface, rather than by slow accumulation of adsorbed CO followed by a “surface explosion” of the reaction. This conclusion is in contrast to the results of the lower pressure measurement by Meißner *et al.*¹⁵ Throughout the oscillations the frequency of the IRAS band characteristic of high rate branch remains approximately constant at a value of 2066 cm⁻¹, but there is a small variation in the frequency of the band associated with the low rate branch around 2081 cm⁻¹. This variation can be assigned the effects of dynamic dipole coupling either through the growth in the size of the CO poisoned (1 × 1) domains (and thus the decreasing proportion of island-edge molecules), or a slight increase in the local coverage.

B. PEEM

The results of repeating the conditions of our IRAS experiments using PEEM are presented in Fig. 9. To relate the setup to the previous PEEM calibration measurements³⁰ and account for day-to-day fluctuations in the measured PEEM intensity, the intensities obtained from a clean surface, a surface of known CO coverage,³² and the O-saturated surface were measured.^{31,32} The numerical values of these average intensities (shown in arbitrary units) are expressed as the darkness, so the value is zero for the clean surface which shows a bright image and is large for the darkest image (corresponding to the largest work function). The value of the saturated oxygen coverage is taken as being 0.7 ML. Following these initial calibration experiments, a partial pressure of CO was introduced and the oxygen partial pressure varied to obtain the reaction conditions corresponding to low rate branch, the high rate branch and pattern formation. The work function increase associated with O adsorption is much larger than that due to CO adsorption (0.8 and 0.15 eV, respectively), so the PEEM intensity is far more sensitive to the presence of oxygen, especially at low coverages. As shown in Fig. 9, the measured PEEM intensity when the

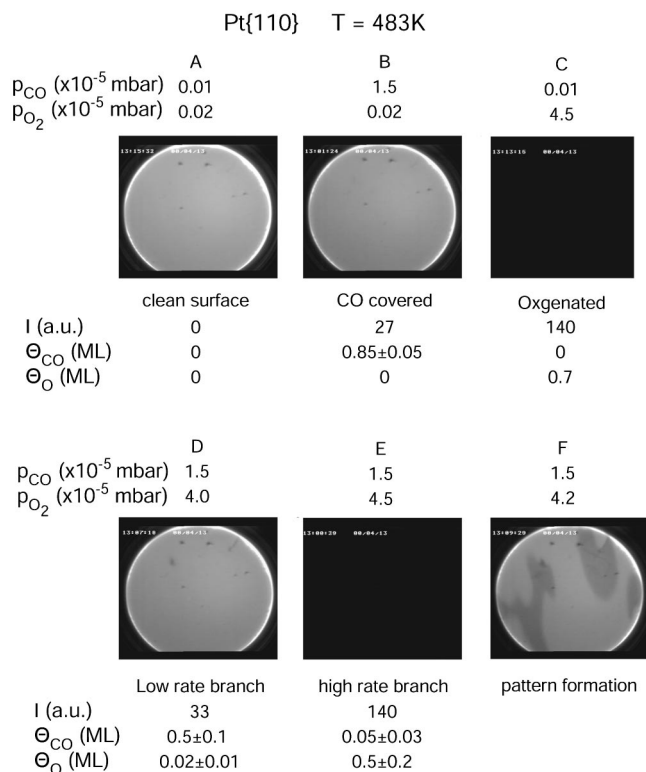


FIG. 9. PEEM images from Pt{110} recorded at 483 K: (A) clean surface; (B) CO-covered surface (exposed to $p_{\text{CO}} = 1.5 \times 10^{-5}$ mbar), 0.85 ML CO (Ref. 64); (C) oxygen-covered surface (exposed to $p_{\text{O}_2} = 4.5 \times 10^{-5}$ mbar); (D) surface undergoing reaction in the high rate branch ($p_{\text{O}_2} = 4.5 \times 10^{-5}$ mbar, $p_{\text{CO}} = 1.5 \times 10^{-5}$ mbar); (E) surface undergoing reaction in the low rate branch ($p_{\text{O}_2} = 4.0 \times 10^{-5}$ mbar, $p_{\text{CO}} = 1.5 \times 10^{-5}$ mbar). Note that the oxygen coverage quoted in this panel of the figure relates to the results of a range of different experiments and not only the specific image shown here; (F) surface undergoing reaction under conditions of pattern formation ($p_{\text{O}_2} = 4.2 \times 10^{-5}$ mbar, $p_{\text{CO}} = 1.5 \times 10^{-5}$ mbar).

surface is entirely reacting under the conditions of the low rate branch [Fig. 9(D)] is almost the same as when the surface is only exposed to CO [Fig. 9(B)]. Furthermore the same intensity is observed in the light patches of the PEEM images during the conditions of pattern formation [Fig. 9(F)]. These results are consistent with the conclusions of our IRAS study that under these conditions the surface is essentially free of adsorbed oxygen. Based on the IRAS data we concluded that in the low reaction rate branch the surface has $\Theta_{\text{CO}} = 0.5 \pm 0.1$ ML and the PEEM intensity then indicates that $\Theta_{\text{O}} = 0.03 \pm 0.01$ ML.

When the surface is reacting in the high rate branch, the IRAS data indicate a CO coverage of only 0.05 ± 0.03 ML, and the small effect which this is expected to have on the numerical value of the PEEM intensity (1.6 ± 1.0 arbitrary units) is clearly an almost negligible contribution to the measured total value of 140 arbitrary units. The dominant intensity change must therefore be ascribed to a high oxygen coverage. The high rate branch is identified as being an oxygenated surface in the (1×2) phase; strictly the results of panels (C) and (E) of Fig. 9 imply an oxygen coverage of $\Theta_{\text{O}} = 0.7$ ML, but the coverage range quoted in Fig. 9 reflects the average of many measurements under different conditions as described below.

The measurements were repeated at different temperatures and pressures ($440 \text{ K} < T < 530 \text{ K}$, 1×10^{-5} mbar $< p_{\text{total}} < 5 \times 10^{-4}$ mbar), both with PEEM and IRAS. Although in IRAS, the same two coverages of CO were observed, and the PEEM intensity of the low rate branch remained constant, the intensity of the high rate branch showed considerable variation under different reaction conditions, and the full range of results of obtained indicate that the high rate branch can correspond to oxygen coverages in the wide range from 0.3–0.7 ML. The large range also reflects not only a real variation in the oxygen coverage but also a reduced precision for the coverage determination when the work function becomes very large and the PEEM intensity is far less sensitive to its exact value. One clear example of the real variation in oxygen coverage in those parts of the surface reacting under the high rate branch conditions can be seen in the PEEM image obtained under the conditions of pattern formation in Fig. 9(F). While the bright regions corresponding to the low rate branch have a brightness very similar to those of panels (B) and (D) as remarked earlier, the dark regions of these images clearly are less dark than in panels (C) and (E), indicating a subsaturation oxygen coverage. This effect has previously been reported in the work function measurements of Eiswirth and Ertl.^{6,7}

We should remark that the variability of the oxygen coverage in the high reaction rate condition and the more constant high CO coverage of the surface in the low rate condition are consistent with expectations based on the site blocking and reconstruction model of the reaction.^{2,18,19,60,67} In this model the low reaction rate condition is attributed to the fact that two neighboring vacant sites are required for molecular oxygen dissociation subsequent atomic oxygen reaction, but a local CO coverage of 0.5 ML blocks adjacent sites and thus inhibits oxygen dissociation and poisons the reaction. In the high rate condition, however, the oxygen steady state coverage simply needs to be sufficient to prevent the coverage of CO rising above the level required to cause statistical nucleation of (1×1) unreconstructed-surface islands.^{68–70}

V. CONCLUSIONS

Our primary objective in this investigation has been to use IRAS, together with some additional PEEM experiments, to obtain quantitative information on the CO and oxygen coverage of a Pt{110} surface as it undergoes an oscillatory CO oxidation reaction, and in particular to provide this characterization of the surface when in the low and high reaction rate branches of this process. Using IRAS to provide this information has required the results of extensive initial calibration experiments to determine how the C–O stretching frequency and integrated absorbance vary as a function of CO coverage, oxygen coadsorption and temperature, and to separate out the roles of dynamic dipole–dipole coupling, chemical shifts and dephasing. In the process of collecting this information, a number of important further results have been obtained. In particular, our results show clearly that CO is distributed rather evenly over the surface at all coverages with and without coadsorbed atomic oxygen, and does not form extended islands. Coadsorption experiments at 300 K

also indicated that there are two different sites for CO adsorption in presence of oxygen. We propose that these may be assigned to CO molecules which adsorb atop hollow and ridge Pt atoms on the (1×2) surface; molecules occupying these two sites may then be rendered inequivalent in terms of oxygen-induced chemical shifts by the specific adsorption sites of the O atoms, probably on the {111}-like trough sides of this missing-row reconstructed surface. We should perhaps note here, however, that under reaction conditions there was no evidence of co-occupation of these two states. The reason for this is not known, but may be related to the significantly higher temperature under reaction conditions which may cause one of these sites to be more strongly favored.

Using the results of these calibration experiments, however, we have also been able to interpret the results of similar studies of the surface under reaction conditions, IRAS providing primary information on the CO coverage and the local coordination site, while PEEM has provided information on the oxygen coverages. Changes on the surface have been related directly to the CO₂ production rate under both steady state and oscillatory reaction conditions. These measurements allow us to clearly exclude some processes which have previously been considered in trying to understand this system. For example, we find no evidence for an oxide phase or subsurface oxygen, nor for any local CO coordination site other than atop (such a bridge).

The CO and oxygen coverages on the Pt{110} surface when undergoing the CO oxidation reaction in both low and high reaction rate branches have been determined. In the low rate branch the surface has a high CO coverage and low oxygen coverage ($\Theta_{\text{CO}} = 0.5 \pm 0.1$ ML, $\Theta_{\text{O}} = 0.03 \pm 0.01$) which must therefore be in the (1×1) unreconstructed phase. By contrast, under high reaction rate branch conditions, the surface has a high oxygen coverage and low CO coverage ($\Theta_{\text{CO}} = 0.05 \pm 0.03$ ML, $\Theta_{\text{O}} = 0.3 - 0.7$ ML) which must therefore be in the reconstructed (1×2) phase. The states observed to make up the high and low reaction branches are responsible for the two main phases observed during pattern formation. These findings are entirely consistent with the site blocking and reconstruction model of the reaction.^{2,18,19,60,67}

Based on this new information and the prior models of the system which are consistent with it, we can relate the two states observed in the hysteresis and in the spatiotemporal pattern formation exhibited by this system as observed by PEEM, IRAS, and LEEM. The high rate phase observed in the (spatio-)temporal pattern formation is an oxygenated (1×2) surface; the low rate corresponds to regions of (1×1) surface with a high (0.5 ML) coverage of CO. The key processes are the role of high CO coverages in blocking sites for O₂ dissociation and the influence of the surface reconstruction and unreconstruction.^{2,15,18,19,60,67} It appears that oxygen dissociation and adsorption is inhibited when $\Theta_{\text{CO}}(\text{local}) > 0.3$ ML and that the reaction is poisoned when $\Theta_{\text{CO}}(\text{local}) = 0.5$ ML; moreover, homogeneous nucleation of the unreconstructed (1×1) phase occurs at $\Theta_{\text{CO}}(\text{local}) = 0.2$ ML and locally these small islands are thought to have a coverage of CO of 0.5 ML. Notice, however, that our IRAS

data are inconsistent with the heterogeneous nucleation and growth of islands of this coverage.

ACKNOWLEDGMENTS

The authors would like to thank F. Meißen and A. Patchett for their close cooperation and useful discussions and likewise the group of H. H. Rotermund.

- ¹R. Imbihl and G. Ertl, *Chem. Rev.* **95**, 697 (1995).
- ²G. Ertl, *Surf. Sci.* **299/300**, 742 (1994).
- ³H. H. Rotermund, *Surf. Sci. Rep.* **29**, 265 (1997).
- ⁴*Oscillations and Traveling Waves in Chemical Systems*, edited by R. J. Field and M. Burger (Wiley, New York, 1985).
- ⁵I. Ferino and E. Rombi, *Catal. Today* **52**, 291 (1999).
- ⁶M. Eiswirth and G. Ertl, *Surf. Sci.* **177**, 90 (1986).
- ⁷M. Eiswirth, Doctorate thesis, University of München, 1987.
- ⁸S. Ladas, R. Imbihl, and G. Ertl, *Surf. Sci.* **198**, 42 (1988).
- ⁹W. Tappe, U. Korte, and G. Meyer-Ehmsen, *Surf. Sci.* **388**, 162 (1997).
- ¹⁰G. Ertl, *Science* **254**, 1750 (1991).
- ¹¹S. Jakubith, H.-H. Rotermund, W. Engel, A. von Oertzen, and G. Ertl, *Phys. Rev. Lett.* **65**, 3013 (1990).
- ¹²A. von Oertzen, A. S. Mikhailov, H. H. Rotermund, and G. Ertl, *J. Phys. Chem. B* **102**, 4966 (1998).
- ¹³K. C. Rose, D. Battogtokh, A. Mikhailov, R. Imbihl, W. Engel, and A. M. Bradshaw, *Phys. Rev. Lett.* **76**, 3582 (1996).
- ¹⁴K. C. Rose, B. Berton, R. Imbihl, W. Engel, and A. M. Bradshaw, *Phys. Rev. Lett.* **79**, 3427 (1997).
- ¹⁵F. Meißen, A. J. Patchett, W. Engel, A. M. Bradshaw, and R. Imbihl (unpublished).
- ¹⁶A. J. Patchett, F. Meißen, W. Engel, R. Imbihl, and A. M. Bradshaw, *Surf. Sci.* **454-456**, 341 (2000).
- ¹⁷M. P. Cox, G. Ertl, and R. Imbihl, *Phys. Rev. Lett.* **54**, 1725 (1985).
- ¹⁸H. P. Bonzel and R. Ku, *Surf. Sci.* **33**, 91 (1972).
- ¹⁹H. P. Bonzel and R. Ku, *J. Vac. Sci. Technol.* **9**, 663 (1972).
- ²⁰G. S. Yablonskii and V. I. Elokhin, in *Perspectives in Catalysis*, edited by J. A. Thomas and K. I. Zamaev (Blackwell Scientific, Boston, 1994).
- ²¹B. C. Sales, J. E. Turner, and M. B. Maple, *Surf. Sci.* **114**, 381 (1982).
- ²²N. A. Collins, S. Sunaresan, and Y. J. Chabal, *Surf. Sci.* **180**, 272 (1987).
- ²³J. H. Miners, R. Martin, P. Gardner, R. Nalezinski, and A. M. Bradshaw, *Surf. Sci.* **377-379**, 791 (1997).
- ²⁴A. M. Bradshaw and E. Schweizer, *Adv. Spectrosc. (N.Y.)* **23**, 413 (1988).
- ²⁵M. Scheffler, *Surf. Sci.* **81**, 562 (1979).
- ²⁶B. N. J. Persson and R. Ryberg, *Phys. Rev. B* **24**, 6954 (1981).
- ²⁷R. K. Sharma, W. A. Brown, and D. A. King, *Surf. Sci.* **414**, 68 (1998).
- ²⁸J. W. Gadzuk and A. C. Luntz, *Surf. Sci.* **144**, 429 (1984).
- ²⁹W. Engel, M. E. Kordes, H. H. Rotermund, S. Kubala, and A. von Oertzen, *Ultramicroscopy* **36**, 148 (1991).
- ³⁰A. von Oertzen, Doctorate thesis, Frei-Universität, Berlin, 1992.
- ³¹S. Cerasari, Doctorate thesis, Frei-Universität, Berlin, 2000 (<http://www.diss.fu-berlin.de/2000/61/indexe.html>).
- ³²S. Cerasari, A. von Oertzen, and H. H. Rotermund (unpublished).
- ³³A. von Oertzen, H. H. Rotermund, and S. Nettesheim, *Surf. Sci.* **311**, 322 (1994).
- ³⁴P. Fery, W. Moritz, and D. Wolf, *Phys. Rev. B* **38**, 7275 (1988).
- ³⁵C. M. Comrie and R. M. Lambert, *J. Chem. Soc., Faraday Trans.* **72**, 1659 (1976).
- ³⁶R. Imbihl, S. Ladas, and G. Ertl, *Surf. Sci.* **206**, L903 (1988).
- ³⁷T. Gritsch, D. Coulman, R. J. Behm, and G. Ertl, *Phys. Rev. Lett.* **63**, 1086 (1989).
- ³⁸B. E. Hayden, A. W. Robinson, and P. M. Tucker, *Surf. Sci.* **192**, 163 (1987).
- ³⁹P. Hofmann, S. R. Bare, and D. A. King, *Surf. Sci.* **117**, 245 (1982).
- ⁴⁰S. Ferrer and H. P. Bonzel, *Surf. Sci.* **119**, 234 (1982).
- ⁴¹P. Hofmann, S. R. Bare, N. V. Richardson, and D. A. King, *Solid State Commun.* **42**, 645 (1982).
- ⁴²M. Nowicki, A. Emundts, G. Pirug, and H. P. Bonzel, *Surf. Sci.* **478**, 180 (2001).
- ⁴³M. I. Ban, M. A. van Hove, and G. A. Somorjai, *Surf. Sci.* **185**, 355 (1987).
- ⁴⁴R. M. Hammaker, S. A. Francis, and R. P. Eischens, *Spectrochim. Acta* **21**, 1295 (1965).
- ⁴⁵G. D. Mahan and A. A. Lucas, *J. Chem. Phys.* **68**, 1344 (1978).

- ⁴⁶S. R. Bare, P. Hofmann, and D. A. King, *Surf. Sci.* **144**, 347 (1984).
- ⁴⁷C. Klünker, M. Balden, S. Lehwald, and W. Daum, *Surf. Sci.* **360**, 104 (1996).
- ⁴⁸C. B. Harris, R. M. Schelby, and P. A. Cornelius, *Phys. Rev. Lett.* **38**, 1415 (1977).
- ⁴⁹B. N. J. Persson, F. M. Hoffmann, and R. Ryberg, *Phys. Rev. B* **34**, 2266 (1986).
- ⁵⁰B. N. J. Persson, *Chem. Phys. Lett.* **149**, 278 (1988).
- ⁵¹E. Schweizer, B. N. J. Person, M. Tüshaus, D. Hoge, and A. M. Bradshaw, *Surf. Sci.* **213**, 49 (1989).
- ⁵²M. Tüshaus, E. Schweizer, P. Hollins, and A. M. Bradshaw, *J. Electron Spectrosc. Relat. Phenom.* **45**, 57 (1987).
- ⁵³H. Conrad, G. Ertl, and J. Küppers, *Surf. Sci.* **76**, 332 (1978).
- ⁵⁴G. E. Thomas and W. H. Wienberg, *J. Chem. Phys.* **70**, 954 (1979).
- ⁵⁵F. M. Hoffman, M. D. Weisel, and C. H. F. Peden, *Surf. Sci.* **253**, 59 (1991).
- ⁵⁶J. Schmidt, Ch. Stuhlmann, and H. Ibach, *Surf. Sci.* **284**, 121 (1993).
- ⁵⁷N. Freyer, M. Kiskinova, G. Pirug, and H. P. Bonzel, *Surf. Sci.* **166**, 206 (1986).
- ⁵⁸A. V. Walker, B. Klötzer, and D. A. King, *J. Chem. Phys.* **109**, 6879 (1998).
- ⁵⁹S. Helveg, H. T. Lorensen, S. Horch, E. Lægsgaard, I. Stensgaard, K. W. Jacobsen, J. K. Nørskov, and F. Besenbacher, *Surf. Sci.* **430**, L533 (1999).
- ⁶⁰T. Engel and G. Ertl, *Adv. Catal.* **28**, 1 (1979).
- ⁶¹M. Peuckert and H. P. Bonzel, *Surf. Sci.* **145**, 239 (1984).
- ⁶²G. Pirug, R. Dziembaj, and H. P. Bonzel, *Surf. Sci.* **221**, 553 (1989).
- ⁶³T. H. Lindstrom and T. T. Tsotsis, *Surf. Sci.* **150**, 487 (1985).
- ⁶⁴D. J. Kaul and E. E. Wolf, *J. Catal.* **91**, 216 (1985).
- ⁶⁵J. Falta, R. Imbihl, M. Sander, and M. Henzler, *Phys. Rev. B* **45**, 6858 (1992).
- ⁶⁶J. Lauterbach and H. H. Rotermund, *Catal. Lett.* **27**, 2 (1994).
- ⁶⁷R. Imbihl, *Prog. Surf. Sci.* **44**, 185 (1993).
- ⁶⁸V. P. Zhdanov, *Surf. Sci.* **426**, 345 (1999).
- ⁶⁹O. Kortlüke, V. N. Kuzovkov, and W. von Neissen, *Phys. Rev. Lett.* **83**, 3089 (1999).
- ⁷⁰O. Kortlüke, V. N. Kuzovkov, and W. von Neissen, *J. Chem. Phys.* **110**, 11523 (1999).